

# Lattice dynamics of $\text{CuGeO}_3$ : inelastic neutron scattering and model calculations

M. Braden<sup>a,b,c,\*</sup>, W. Reichardt<sup>a</sup>, B. Hennion<sup>b</sup>, G. Dhalenne<sup>d</sup>, A. Revcolevschi<sup>d</sup>

<sup>a</sup> *Forschungszentrum Karlsruhe, IFP, Postfach 3640, D-76021 Karlsruhe, Germany*

<sup>b</sup> *Laboratoire Léon Brillouin, C.E.A./C.N.R.S., F-91191-Gif-sur-Yvette CEDEX, France*

<sup>c</sup> *II. Phys. Inst., Univ. zu Köln, Zùlpicher Str. 77, D-50937 Köln, Germany*

<sup>d</sup> *Laboratoire de Physico-Chimie de l'Etat Solide, Université Paris Sud, 91405 Orsay Cedex, France*

(Dated: February 1, 2008)

The lattice dynamics in  $\text{CuGeO}_3$  has been analyzed by the combination of inelastic neutron scattering studies and lattice dynamical model calculations. We report an almost complete set of dispersion curves along the three orthorhombic directions and along [101]. The dispersion of branches associated with the modes directly involved in the spin-Peierls transition allows to explain the particular propagation vector of the structural distortion in the dimerized phase.

PACS numbers: 75.40.Gb, 61.12.Ex, 63.20.-e

## I. INTRODUCTION

The spin-Peierls transition in  $\text{CuGeO}_3$  has attracted considerable interest due to the relatively simple crystal structure of this material allowing experimental studies so far not possible in the organic spin-Peierls compounds<sup>1</sup>. In particular neutron scattering and diffraction techniques could be used for the study of this material<sup>2,3,4</sup>.

The spin-Peierls transition is based on magneto-elastic coupling : the dimerization of the magnetic chain results from the structural distortion. Since the gain in magnetic energy is linear, and since the loss in elastic energy is quadratic in the distortion, in a simple one-dimensional picture the combined structural and magnetic transition must occur. In real systems inter-chain coupling may, however, favor three-dimensional antiferromagnetic ordering.

In  $\text{CuGeO}_3$ , the microscopic coupling has been clarified by experimental – magnetic and structural – and theoretical studies in great detail. The spin-1/2 chains in  $\text{CuGeO}_3$  are formed by the  $\text{CuO}_2$ -chains characterized by edge sharing  $\text{CuO}_4$ ; the oxygen in these chains is labeled  $\text{O}^{25}$ . These chains are directly connected in the  $b$ -direction by  $\text{GeO}_4$ -tetrahedra. In contrast, the coupling along  $a$  through the apical oxygen,  $\text{O1}$ , is only weak due to the long  $\text{CuO1}$ -distance. A detailed description of the crystal structure and its temperature dependence is given in references<sup>6,7</sup>. The variation of the magnetic interaction parameter,  $J$ , in the spin-Peierls phase results mainly from the modulation of the  $\text{Cu-O-Cu}$  bond-angle,  $\eta$ , which in contrast to the high  $T_c$  superconductor parent compounds is close to  $90^\circ$ <sup>6,8</sup>. In an isolated  $\text{CuO}_2$ -chain with  $90^\circ$  bond angle, there should be no antiferromagnetic exchange, since two exchange-paths cancel each other. In  $\text{CuGeO}_3$  the exact cancellation of these rather large values is destroyed by the deviation of the bond-angle from  $90^\circ$  and by the hybridization with the Ge-atoms acting as side-groups. This renders the magnetic interaction quite sensitive to small structural changes. Already in the non-dimerized phase the magneto-elastic coupling causes anomalous temperature dependences via

the equilibrium of magnetic and structural energy<sup>7,9</sup>. In the spin-Peierls phase the dimerization is achieved by the modulation of both the  $\text{Cu-O-Cu}$  bond angle  $\eta$ , and the angle between the  $\text{CuO}_2$ -ribbons and the  $\text{Ge-O1}$ -bond,  $\delta^6$ . The quantitative relation between the bond angles and  $J$  has been calculated by several techniques : on the base of band structure calculations<sup>6,8,10</sup>, from thermodynamic considerations<sup>11</sup> and within a RPA-theory of the spin-Peierls transition<sup>12</sup>. A comparative discussion of the distinct techniques is given in ref.<sup>12</sup>.

It is obvious that phonons play an important role in any spin-Peierls transition. Therefore, the lattice dynamics of  $\text{CuGeO}_3$  has been studied by several techniques. Due to its transparency  $\text{CuGeO}_3$  presents favorable conditions for optical methods; almost all zone-center frequencies have been determined by the combination of Raman and Infrared studies<sup>13</sup>. However, the spin-Peierls transition is characterized by a breaking of translational symmetry, therefore, the phonons directly involved in the transition must have propagation vectors away from  $\Gamma$ . In  $\text{CuGeO}_3$  the lattice is doubled along  $a$  and  $c$ , the propagation vector is, hence,  $(0.5 \ 0 \ 0.5)$ . Several groups have challenged the question whether the involved phonon modes soften close to the transition or not by inelastic neutron scattering<sup>14,15,16</sup>. These studies tried to solve the problem by measuring only a few branches, which does not allow to characterize the lattice dynamics of this complex system.  $\text{CuGeO}_3$  has 10 atoms in its primitive cell, the associated lattice dynamics with its 30 phonon branches is close to the maximum complexity one may treat today. The identification of the involved phonon modes could be achieved only by the complete study reported here.

We have already published results concerning the phonon modes directly related to the spin-Peierls transition<sup>17</sup>. There are four modes with the symmetry of the transition from  $\text{Pbmm}$  to  $\text{Bbcm}$ . Two aspects of these modes were unexpected. First, the distortion of the dimerized phase does not correspond to just one of these modes, but at least two polarization patterns have to be combined. Second, the two strongly involved modes do not soften close to the transition in contradiction with the

Cross-Fisher prediction<sup>18</sup>. These results have stimulated new theoretical studies : Gros and Werner have extended the Cross-Fisher theory in order to explain the missing of phonon softening<sup>19</sup> and Uhrig<sup>20</sup> has stressed the importance of the high phonon frequencies compared to the magnetic energy scale, i.e. a non-adiabatic condition. In general it has been shown that coupling of the spin system with a branch of phonons is important for a quantitative understanding of the spin-Peierls transition<sup>21,22</sup>.

In this paper we want to present the general lattice dynamical study furnishing the basis for the identification of the relevant phonon modes. Only the combination of neutron scattering with lattice dynamical calculations permits to treat a phonon problem of this complexity. CuGeO<sub>3</sub> is one of the few complex systems where the lattice dynamics may be considered as being understood in detail. In this sense it is a rather promising material for validating ab-initio procedures to calculate phonon frequencies, so far restricted to less complex systems. In addition, the lattice dynamics of CuGeO<sub>3</sub> presents several aspects not related to the spin-Peierls scenario but interesting in themselves. Furthermore, the phonon dispersion of CuGeO<sub>3</sub> should have some exemplary character for the wide class of silicates and germanates<sup>23</sup> and also for other cuprate chain systems of current interest.

In section II we describe the neutron scattering studies and present the lattice dynamics of CuGeO<sub>3</sub>. The phenomenological model used to accompany the measurements and to interpret the data is introduced in section III. The general discussion of the phonon dispersion in CuGeO<sub>3</sub> based on the experimental studies and the model is given in section IV. In section V we give some further information on the modes directly involved in the transition which is not included in our previous paper. Finally, in section VI, we briefly discuss the possibility of distinct structural order parameters.

## II. INELASTIC NEUTRON SCATTERING STUDIES

The main part of the studies of the phonon dispersion has been performed on the triple axis spectrometer 1Ta, operated by the Forschungszentrum Karlsruhe at the Orphée reactor in Saclay. A few additional studies have been made on the spectrometer 2T also installed at the Orphée reactor<sup>24</sup>.

Since it has been necessary to study the phonon dispersion in CuGeO<sub>3</sub> in its entity, the amount of beam time spent on this problem was considerable. 25 days on 1T and 7 days on 2T were used in order to determine an almost complete set of phonon branches along the three orthorhombic directions and along [101]. For the study of the temperature dependence of modes relevant to the spin-Peierls transition, another 8 days were used on 1Ta.

For a first experiment, two crystals of 550 mm<sup>3</sup> volume each have been coaligned in the [100]/[001]-orientation using a double goniometer. Due to the long *b*-axis this

orientation allows attaining Q-values out of the scattering plane by tilting the sample with the goniometer. Along the [100]-direction almost all modes could be determined in this orientation. One of the two crystals shows a larger mosaic spread around *a*, which was tolerable in the [100]/[001]-orientation since it becomes hidden by the large vertical divergence. For orientations with *a* not parallel to the scattering plane it has been advantageous to use only one crystal. Further experiments were performed in the [010]/[001]-, [100]/[010]- and [101]/[010]-orientations.

For all measurements a pyrolytic graphite (PG) analyzer was used; in the low frequency range up to ~10THz a PG-(002) monochromator and, at high frequencies, a Cu-(111) monochromator. For a few studies requiring an exceptional resolution a Cu-(220) monochromator was mounted. Due to double focusing arrangement of monochromators and analyzers the spectrometer 1T yields a considerable gain in intensity<sup>25</sup>. The focusing arrangement is incompatible with the use of collimators but yields a better resolution in comparison to a configuration with flat crystals and open collimations. Roughly, the focusing configuration corresponds to a conventional spectrometer with 37'-collimators throughout. All scans were performed with the final energy fixed in the neutron energy loss mode and, apart a few scans aiming at acoustic phonons, the final energy was fixed to the values of 3.555 and 7.37THz, where higher order contaminations may be suppressed by the PG filter.

The phonon dispersion was studied mainly at room temperature; just for the highest frequency modes it has been favorable to cool the sample to 10K in order to reduce the background.

In figure 1 we show typical phonon scans which illustrate the different effort to be made to analyze phonon frequencies at low and high energy. The intensity, *I*, of a one phonon process in neutron energy loss mode is given by<sup>26</sup>:

$$I \propto \frac{1}{\omega} \cdot (n(\omega) + 1) \left\{ \sum_d \frac{b_d}{\sqrt{m_d}} \cdot e^{(-W_d + i\mathbf{Q} \cdot \mathbf{r}_d)} \cdot (\mathbf{Q} \cdot \mathbf{e}_d) \right\}^2 \quad (1),$$

( $\omega$  denotes the phonon frequency,  $\mathbf{q}$  the wave-vector,  $\mathbf{Q} = \mathbf{g} + \mathbf{q}$  the scattering vector ( $\mathbf{g}$  the reciprocal lattice vector)  $e^{-W_d}$  the Debye-Waller-factor, and the sum extends over the atoms in the primitive cell with mass  $m_d$  scattering length  $b_d$ , position  $\mathbf{r}_d$  and polarization vector  $\mathbf{e}_d$ . In general, the intensity is determined by the Bose-factor,  $n(\omega)$ , and the  $\frac{1}{\omega}$ -term, which strongly reduce the effectiveness to observe high energy modes. In analogy to the elastic structure factor, the sum in (1) is called dynamic structure factor; it describes the interference of the interaction of the distinct atoms weighted by the scalar product of their displacements with the scattering vector  $\mathbf{Q}$ . Only phonons with some polarization parallel to  $\mathbf{Q}$  can be observed. The right side of equation (1) may be calculated with a lattice dynamical model in order to

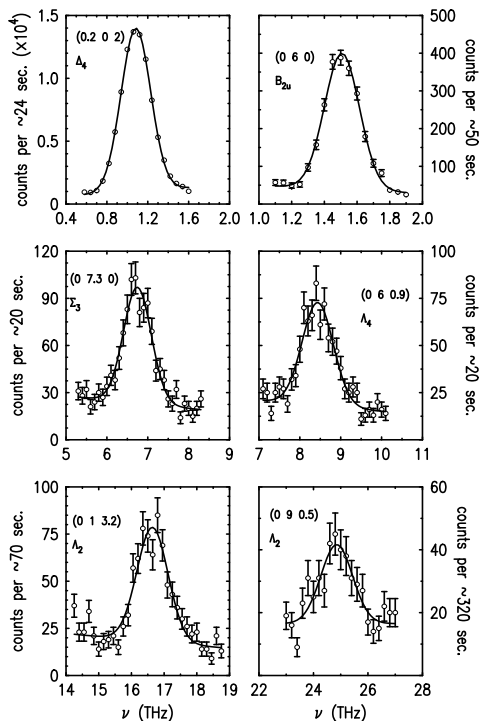


FIG. 1: Exemplary scans aiming at determining phonon frequencies at the  $\Gamma$ -point and in the Brillouin-zone with fits by Gaussian profiles and sloping background.

predict favorable conditions for the measurement and in order to identify single phonon modes.

Figure 1 shows a scan across a transverse acoustic phonon at  $\mathbf{g}=(0\ 0\ 2)$  (upper left); the mode is polarized along the  $c$ -direction. This mode yields a high peak intensity in accordance with the strong  $(0\ 0\ 2)$  Bragg-reflection intensity. In contrast, the determination of the highest frequencies requires an extreme effort in beam-time; the figure 1 (lower right) presents results for a strong dynamic structure factor; modes with unfavorable structure factors may not be analyzed in practice in this frequency region. In the medium energy range the analysis of the phonon spectra is dominated by the question whether the modes may be isolated for a certain  $\mathbf{Q}$ -value.

The phonon frequencies were obtained by fitting Gaussian distributions to the measured profiles. This procedure may be used in principle only when the curvature of the dispersion surface can be neglected in the range of the four-dimensional resolution ellipsoid. The whole set of dispersion curves along the orthorhombic directions, given in figure 2, is separated according to the irreducible representations. Only a few high energy branches were not studied in our experiments; however, their zone center frequencies are fixed by the optical techniques and the dispersion is most likely flat.

### III. LATTICE DYNAMICAL MODEL CALCULATIONS FOR $\text{CuGeO}_3$

In order to analyze a complex problem like the phonon dispersion it is essential to take profit of symmetry considerations. The 10 atoms in the primitive cell correspond to 30 zone-center frequencies characterized by their polarization vectors. The symmetry of the  $\text{CuGeO}_3$  crystal structure allows a separation corresponding to irreducible representations<sup>27</sup> each of them being characterized by a certain polarization scheme. The  $\Gamma$ -modes may be divided into :  $4A_g + 2A_u + B_{1g} + 6B_{1u} + 4B_{2g} + 6B_{2u} + 3B_{3g} + 4B_{3u}$ . The schemes of the polarization patterns are given in Table I; they result from the crystal symmetry.  $A_g$  modes show the full symmetry, their displacement parameters hence correspond to the free parameters in the  $\text{CuGeO}_3$  structure, Ge-x, O1-x, O2-x and O2-y.  $A_u$ -modes show displacements of Cu and O2 along  $c$ ; they are silent since shifts in neighboring chains cancel each other.  $B_{iu}$  are characterized by displacements of all atoms in the  $i$ -direction with in-phase shift of equivalent atoms; in particular they contain the starting points of the acoustic branches.  $B_{ig}$ -modes are even modes which break a two-fold axis.

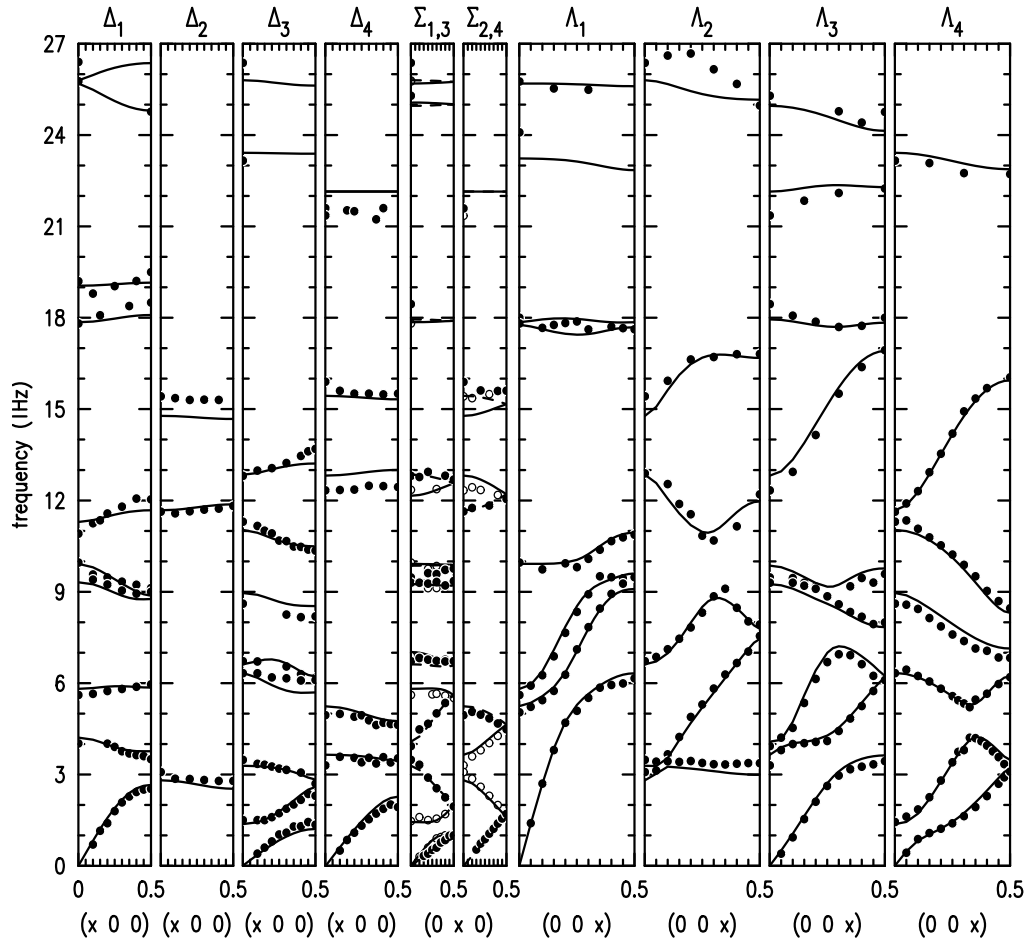


FIG. 2: Phonon dispersion in CuGeO<sub>3</sub>: branches are separated according to irreducible representations along the three orthorhombic directions; circles denote experimental points (open circles along (0x0)  $\Sigma_1$ - and  $\Sigma_2$ -modes) and lines the frequencies calculated by the model.

	Cu (.5 0 0)	Cu' (.5 .5 0)	Ge (.07 .25 .5)	Ge' (-.07 .75 .5)	O1 (.87 .25 0)	O1' (-.87 .75 0)	O2 (.28 .08 .5)	O2' (-.28 -.08 .5)	O2'' (-.28 .58 .5)	O2''' (.28 .42 .5)
6 B <sub>1u</sub>	A B 0	A-B 0	C 0 0	C 0 0	D 0 0	D 0 0	E F 0	E F 0	E-F 0	E-F 0
6 B <sub>2u</sub>	A B 0	-A B 0	0 C 0	0 C 0	0 D 0	0 D 0	E F 0	E F 0	-E F 0	-E F 0
4 B <sub>3u</sub>	0 0 A	0 0 A	0 0 B	0 0 B	0 0 C	0 0 C	0 0 D	0 0 D	0 0 D	0 0 D
4 A <sub>g</sub>	0 0 0	0 0 0	A 0 0	-A 0 0	B 0 0	-B 0 0	C D 0	-C-D 0	-C D 0	C-D 0
4 B <sub>2g</sub>	0 0 0	0 0 0	0 A 0	0-A 0	0 B 0	0-B 0	C D 0	-C-D 0	C-D 0	-C D 0
2 A <sub>u</sub>	0 0 A	0 0-A	0 0 0	0 0 0	0 0 0	0 0 0	0 0 B	0 0 B	0 0-B	0 0-B
3 B <sub>3g</sub>	0 0 0	0 0 0	0 0 A	0 0-A	0 0 B	0 0-B	0 0 C	0 0-C	0 0-C	0 0 C
1 B <sub>1g</sub>	0 0 0	0 0 0	0 0 0	0 0 0	0 0 0	0 0 0	0 0 A	0 0-A	0 0 A	0 0-A
10 Δ <sub>1</sub>	A B 0	A-B 0	C 0 0	D 0 0	E 0 0	F 0 0	G H 0	I J 0	I-J 0	G-H 0
3 Δ <sub>2</sub>	0 0 A	0 0-A	0 0 0	0 0 0	0 0 0	0 0 0	0 0 B	0 0 C	0 0-C	0 0-B
10 Δ <sub>3</sub>	A B 0	-A B 0	0 C 0	0 D 0	0 E 0	0 F 0	G H 0	I J 0	-I J 0	-G H 0
7 Δ <sub>4</sub>	0 0 A	0 0 A	0 0 B	0 0 C	0 0 D	0 0 E	0 0 F	0 0 G	0 0 G	0 0 F
10 Σ <sub>1</sub>	A B 0	-A B 0	C D 0	-C D 0	E F 0	-E F 0	G H 0	I J 0	-G H 0	-I J 0
5 Σ <sub>2</sub>	0 0 A	0 0-A	0 0 B	0 0-B	0 0 C	0 0-C	0 0 D	0 0 E	0 0-D	0 0-E
10 Σ <sub>3</sub>	A B 0	A-B 0	C D 0	C-D 0	E F 0	E-F 0	G H 0	I J 0	G-H 0	I-J 0
5 Σ <sub>4</sub>	0 0 A	0 0 A	0 0 B	0 0 B	0 0 C	0 0 C	0 0 D	0 0 E	0 0 D	0 0 E
8 Λ <sub>1</sub>	0 0 A	0 0 A	B 0 C	-B 0 C	D 0 E	-D 0 E	F G H	-F-G H	-F G H	F-G H
2 Λ <sub>2</sub>	0 0 A	0 0-A	0 B 0	0-B 0	0 C 0	0-C 0	D E F	-D-E F	D-E-F	-D E-F
9 Λ <sub>3</sub>	A B 0	A-B 0	C 0 D	C 0-D	E 0 F	E 0-F	G H I	G H-I	G-H-I	G-H I
7 Λ <sub>4</sub>	A B 0	-A B 0	0 C 0	0 C 0	0 D 0	0 D 0	E F G	E F-G	-E F G	-E F-G
17 X0X <sub>1</sub>	A B C	A-B C	D 0 E	F 0 G	H 0 I	J 0 K	L M N	O P Q	O-P Q	L-M N
13 X0X <sub>2</sub>	A B C	-A B-C	0 D 0	0 E 0	0 F 0	0 G 0	H I J	K L M	-K L-M	-H I-J
4 T <sub>2</sub> <sup>+</sup>	0 0 A	0 0 -A	0 B 0	0 -B 0	0 0 0	0 0 0	C D 0	C D 0	-C D 0	-C D 0

TABLE I: Polarization schemes according to the crystal structure of CuGeO<sub>3</sub> for all  $\Gamma$ -modes and for the representations along the three orthorhombic directions and along  $[101]$  and for the T<sub>2</sub><sup>+</sup>-modes associated with the spin-Peierls transition at  $\mathbf{q}=(0.5\ 0\ 0.5)$ ; the first lines give the positions of 10 atoms forming a primitive unit, the following lines show the displacements of these atoms. A letter at the  $i$ -position, signifies that this atom is moving along the  $i$ -direction, a second appearance of the same letter signifies that the second atom moves with the same amplitude ("-" denotes a phase shift) in the corresponding direction.

10 $\Delta_1 : 4 A_g + 6 B_{1u}$	10 $\Delta_3 : 4 B_{2g} + 6 B_{2u}$
3 $\Delta_2 : 2 A_u + B_{1g}$	7 $\Delta_4 : 3 B_{3g} + 4 B_{3u}$
10 $\Sigma_1 : 4 A_g + 6 B_{2u}$	10 $\Sigma_3 : 4 B_{2g} + 6 B_{1u}$
5 $\Sigma_2 : 2 A_u + 3 B_{3g}$	5 $\Sigma_4 : B_{1g} + 4 B_{3u}$
8 $\Lambda_1 : 4 A_g + 6 B_{3u}$	9 $\Lambda_3 : 3 B_{3g} + 6 B_{1u}$
6 $\Lambda_2 : 2 A_u + 4 B_{2g}$	7 $\Lambda_4 : B_{1g} + 6 B_{2u}$
17 X0X <sub>1</sub> : 8 $\Lambda_1 + 9 \Lambda_3$ : 4 $A_g + 6 B_{3u} + 3 B_{3g} + 6 B_{1u}$	
13 X0X <sub>2</sub> : 6 $\Lambda_2 + 7 \Lambda_4$ : 2 $A_u + 4 B_{2g} + B_{1g} + 6 B_{2u}$	

TABLE II: Compatibility relations in CuGeO<sub>3</sub>

In an analogous way the crystal symmetry allows also to divide the phonon polarization patterns for any  $\mathbf{q}$ -value at high symmetry points or lines in the Brillouin-zone, in particular along the three orthorhombic directions:  $\Delta$  corresponds to  $[x00]$ ,  $\Sigma$  corresponds to  $[0x0]$  and  $\Lambda$  corresponds to  $[00x]$ . The separation of the 30 branches according to four distinct representations is an important simplification for the analysis of the phonon dispersion as it may already be seen in figure 2.

In the definition used here, the  $X_1$ -representation always contains the longitudinal acoustic modes with  $X=\Delta, \Sigma$  or  $\Lambda$ . The  $X_2$ -representation is characterized by the fact that no acoustic modes correspond to it, and  $X_3$ - and  $X_4$ -representations are given by the transverse acoustic branches in the sequence of the polarizations, along  $a$  before along  $b$  before along  $c$ . The polarization patterns according to these representations are given in Table I for the main symmetry directions and for  $[X0X]$ . The division according to the representations has significance for the neutron scattering intensity : they yield selection rules for the observation of the modes which allow an identification. The relations between the irreducible representation at  $\Gamma$  and in the zone are given by the compatibility relations shown in Table III. For instance  $A_g$ -modes always correspond to the  $X_1$ -representation and the  $A_u$  to the  $X_2$ -representation. Since CuGeO<sub>3</sub> is an insulator, polar modes exhibit Lydane-Sachs-Teller (LST) splitting, the longitudinal frequencies correspond to starting points of  $X_1$ -branches with  $X$  being the polarization direction, and the transverse frequencies to the  $X_3$  and  $X_4$ -branches. The symmetry further leads to a degeneration at  $\mathbf{q}=(0\ 0.5\ 0)$ , where a  $\Sigma_1$ -branch connects with a  $\Sigma_3$ -branch and where a  $\Sigma_2$ -branch connects with a  $\Sigma_4$ -branch.

In the frame of harmonic lattice dynamics one may reduce the equations of movement to a 3n-dimensional Eigen-value problem for each allowed  $\mathbf{q}$ -value, see references<sup>28,29</sup>,  $\omega^2 \mathbf{e} = \bar{D} \mathbf{e}$ ; here  $\mathbf{e}$  is the 3n-dimensional Polarization vector and  $D$  the dynamical matrix given by :

$$D_{\alpha,\beta}(d,d') = \frac{1}{(m_d m_{d'})^{1/2}} \sum_{l'} \Phi_{\alpha,\beta}(0d,l'd') \exp(iql') \quad (2).$$

Here the indices  $l'$  numerate the cells,  $d,d'$  the atoms within one cell, and  $\alpha,\beta$  the three space directions.  $\Phi_{\alpha,\beta}(0d,l'd')$  are the force constants between the atoms  $d$  and  $d'$  in cells shifted by  $l'$  corresponding to the directions  $\alpha$  and  $\beta$ . The determination of the force constants is the central problem to analyze the phonon dispersion.

For the description of the phonon dispersion in CuGeO<sub>3</sub> we use Coulomb-potentials with effective charges,  $V(r) \propto \frac{Z_1 Z_2 e^2}{r}$  and the repulsive forces are described by Born-Mayer potentials  $V(r) = A \cdot \exp(-r/r_0)$ . Shell charges describing a single-ion polarizability have been introduced for all atoms with a single shell-core force constant. The interatomic forces act on the shells in our model. Chaplot et al.<sup>30</sup> have reported a common model for compounds related to the high- $T_c$  superconducting cuprates; these Cu-O-parameters have been used as starting values for the description of CuGeO<sub>3</sub>. The model has been initially adapted to the optical frequencies and has been continuously refined with the inelastic neutron scattering results. The parameters have been fitted to the observed phonon frequencies and to zero forces on the atoms in the equilibrium positions. In addition, the predictions of the model concerning the dynamic structure factors have been compared to the measured intensities. All calculations were performed with the GENAX program<sup>31</sup>.

We found that several features of the phonon dispersion could only be reproduced by the inclusion of angular forces for the Ge-O-interaction. The angular forces,  $\frac{d^2 V}{d\alpha^2}$ , are divided by the lengths of the two distances, in order to yield values comparable to usual force constants. The angular forces at the Ge-site reflect the strong covalent character of these bonds and are expected. However, also an angular force in the Cu-O-arrangement gave a significant improvement, whereas, in the HTSC cuprates no such parameters are needed.

The angular forces, however, interfere with the forces arising from the Born-Mayer potentials. Therefore, it is impossible to describe all identical pairs by a single potential. In a first model, model I see Table III, additional force constants were introduced for nearest neighbors, the forces acting in this model correspond hence to the sum of the direct force constants plus the contribution from the Born-Mayer potentials. The Cu-O2 potential as well as the van der Waals terms were completely dropped in this model. Model I gives a very good description of the frequency data : the entire set of over 700 phonon frequencies is described with a mean deviation of 0.19 THz. We then attempted to simplify the model by limiting the amount of force constants, model II in Table III. Only nearest neighbor Ge-O interaction is described by force constants, all other forces are deduced from potentials. In addition O-O van der Waals terms and another angular force were introduced. This model too gives a satisfactory description of the frequency data, mean deviation of 0.21 THz, but the the equilibrium forces on the atoms are much higher.

ionic part						
model I				model II		
ion	Z	Y	K	Z	Y	K
Cu	1.77	4.0	2.8	1.87	3.91	2.0
Ge	2.26	0.0	/	1.836	0.0	/
O1	-1.22	-2.8	2.0	-1.03	-2.18	1.8
O2	-1.41	-3.3	2.0	-1.34	-3.14	1.8

potentials						
model I				model II		
pair	A(eV)	r <sub>0</sub> (Å)		A(eV)	r <sub>0</sub> (Å)	
Cu-O1	900	0.305		1008	0.305	
Cu-O2	/	/		4294	0.226	
Ge-O	2500	0.243		/	/	
O1-O1	1300	0.288		2000	0.284	
O1-O2	1800	0.288		2000	0.284	
O2-O2	1500	0.288		2000	0.284	

force constants (dyn/cm)				
pair	F	G	F	G
Ge-O2	98846	30082	603041	-53026
Ge-O1	2233	31133	470090	-37047
Cu-O2	262013	-29617		
O2-O2 (in CuO <sub>4</sub> )	-15963	4619		
O1-O2	5202	-4591		
O2-O2 (in GeO <sub>4</sub> )	16428	-8400		

angular force constants (dyn/cm)		
O1-Ge-O2	2523	8776
Cu-O2-Ge	1705	4936
Ge-O1-Ge	10816	19754
O2-Cu-O2	3753	3921
O2-Ge-O2	/	10897

TABLE III: Model parameters for the description of the phonon dispersion in CuGeO<sub>3</sub>; for the explanation of the parameters see text; Z,Y are in electron charges; K in 10<sup>6</sup>dyn/cm; in model II the uniform O-O potentials contains also a van der Waals term  $-30(\text{ev } \text{\AA}^6) \cdot r^{-6}$  with  $r$  the interatomic distance in Å.

Both CuGeO<sub>3</sub>-models present ionic charges much lower than the chemical values, as it is typically observed. The strong reduction, at least in case of Ge, is certainly caused by strong covalence of the bonds. The shell charges and forces, however, could be chosen similar to values found in other materials<sup>30</sup>. Due to its better description, we discuss only the results of model I in the following.

	Popovic et al.	neutrons	Udagawa et al.	calculation
A <sub>g</sub>	5.606	5.532	5.516	5.81
	9.953	9.692	9.923	9.92
	17.808	18.13	17.78	17.85
	25.753	/	25.723	25.69
B <sub>1g</sub>	11.632	11.68	11.512	11.68
B <sub>2g</sub>	3.478	3.46	3.388	3.29
	6.716	6.86	6.626	6.62
	12.801	12.95	12.92	12.85
	26.352	26.71	26.382	25.80
B <sub>3g</sub>	3.298	3.441	3.298	3.65
	12.322	12.34	12.292	12.82
	21.345	/	21.376	22.14

TABLE IV: Comparison of the Raman-results by Udagawa et al.<sup>32</sup> and by Popovic et al.<sup>13</sup> with the frequencies determined by inelastic neutron scattering and calculations with the lattice dynamical model, all values are given in THz.

#### IV. DISCUSSION OF THE PHONON DISPERSION IN CUGEO<sub>3</sub>

Several groups have performed Raman-studies on CuGeO<sub>3</sub>; the agreement between these results is good<sup>13,32,33,34</sup>. In Table IV we compare the results of Udagawa et al.<sup>32</sup> and Popovic et al.<sup>13</sup> with the values obtained by inelastic neutron scattering and the frequencies calculated with the model. The experimental values agree within 2% and also the agreement with the model is satisfactory, except for the Ge-O-bond stretching vibrations. The latter failure is certainly due to the insufficient description of the covalent Ge-O-bonds; within the parameter range a better description may be obtained but at expense of the low frequency agreement.

Infrared-studies on CuGeO<sub>3</sub> were reported by several groups<sup>13,33,35,36,37,38,39</sup>, whose results correspond well for modes polarized along  $b$  and  $c$ . The determination of the frequencies for modes polarized along  $a$  is hampered by the shape of the crystal and was attempted only by one group<sup>13</sup>. Table V compares the optical results with the neutron and model frequencies; there is only one discrepancy concerning an  $a$ -polarized mode.

Popovic et al. have interpreted a weak signal near 480cm<sup>-1</sup> or 14 THz as a B<sub>1u</sub>-mode. This frequency is, however, not in accordance with the lattice dynamical calculations. The determination of the LST-splitting by inelastic neutron scattering is in general difficult, since the extension of the four-dimensional resolution ellipsoid always favors the observation of the transverse modes. For this reason there is little chance to determine the LO-frequency if the LST-splitting is comparable or smaller than the resolution. Therefore, we have attempted the measurement of the longitudinal polar frequencies only for a few favorable cases. Figure 3 shows an energy scan across the B<sub>3u</sub> pair at 15.7-17.3 THz; these frequencies

	Popovic et al. TO/LO	neutrons	calculation
$B_{1u}$	3.927 4.017	4.16 /	4.081 4.212
	9.833 11.153	9.3 9.6	9.252 9.312
	14.33 14.66	9.47 10.91	9.860 11.294
	18.438 19.182	18.24 /	17.945 19.052
$B_{2u}$	24.07 25.27	/ /	24.960 25.800
	1.439 1.469	1.508 /	1.370 1.438
	6.326 6.925	6.372 /	6.335 7.023
	8.544 9.234	8.58 /	8.961 9.419
$B_{3u}$	11.302 12.412	11.41 /	11.03 12.156
	23.145 25.693	/ /	23.42 25.068
	4.947 5.037	5.109 /	5.239 5.249
	15.869 17.990	15.73 17.27	15.435 17.77
$A_u$	21.586 24.074	/ /	22.15 23.23
	/	3.081	2.811
	/	15.42	14.77

TABLE V: Comparison of the infrared-results by Popovic et al.<sup>13</sup> with the inelastic neutron results and calculated frequencies, TO and LO denote the transverse and longitudinal optic frequencies, respectively, in THz.

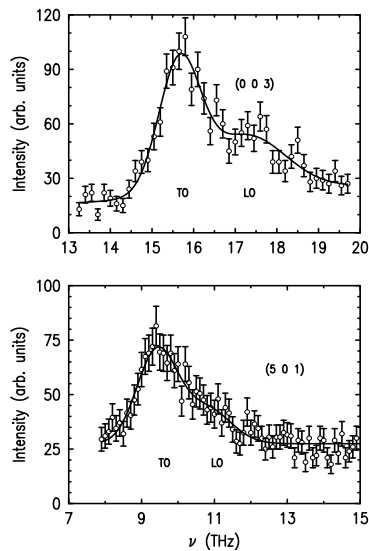


FIG. 3: Scans across polar modes: above  $B_{3u}$  pair, below  $B_{1u}$ -pair.

confirm the infrared results. In the lower scan one expects the  $B_{1u}$ -mode, assumed by Popovic et al.<sup>13</sup> near 14 THz. Unambiguously, this scan reveals a lower energy for this mode, in good agreement with the model calculations. From this scan and from the extrapolation of the branches starting at this mode, we conclude that the TO- and LO-frequencies of the third highest  $B_{1u}$ -mode amount to 9.47 and 10.91 THz. The next lower  $B_{1u}$ -mode is found at 9.3–9.6 THz, hence there is an overlap of these two pairs, which will produce a single plateau in the reflectivity spectra at 9–11 THz, in addition this

mode possesses little oscillator strength. Indeed we may describe the spectrum observed by Popovic et al.<sup>13</sup> reasonably well on the basis of these frequencies.

The crystal symmetry only yields the schemes of the polarization patterns as given in Table I. For any representation with a multiplicity higher than one, one has to know the force constants in order to determine the polarization patterns. Figure 6 shows the polarization patterns calculated with the lattice dynamical model. Similar results were also reported by Popovic et al.<sup>13</sup>; small deviations are probably due to the misinterpretation of the  $B_{1u}$ -mode.

The  $A_u$ -modes correspond to displacements of the Cu and O2 positions along  $c$ . The mode with an opposite shift causes significant alternation of the Cu-O2-bond distance, this mode has a high frequency of 15.4 THz. The in-phase vibration, where the entire ribbons are shifted along  $c$ , is low in frequency at 3.1 THz. The distortion in the spin-Peierls phase is related to both  $A_u$ -modes.

The rotation of the  $\text{CuO}_2$ -ribbons around the  $c$ -axis corresponds to the  $A_g$ -mode at 9.9 THz. This high frequency may surprise in view of the fact that the ribbons rotate as function of temperature around  $c$ .<sup>7</sup> The polarization pattern of the 9.9 THz-mode lacks the alternation of the  $b$ -lattice constant and the associated shift of the  $\text{GeO}_4$ -tetrahedra; without these elements the vibration is hence rather hard.

Several modes correspond to rotations of the tetrahedron chains around the  $c$ -axis. The  $B_{2g}$ -mode at 6.7 THz may be described by the rotation around an axis near the middle of the O2-O2-edges; this vibration is rather hard. The  $B_{2g}$ -mode at 3.5 THz, in contrast, corresponds to the rotation around the O1-O1-line and is hence related to the distortion in the spin-Peierls phase. In this low frequency  $B_{2g}$ -mode neighboring tetrahedra rotate in the same sense, and the corresponding anti-phase rotation is approximatively realized in the  $B_{2u}$ -modes at 6.3 and 1.5 THz. The pure anti-phase tetrahedron rotation is not an Eigen-mode due to the stronger influence of the CuO-forces; the difference between the two  $B_{2u}$  modes concerns just the Cu-shift.

Modes with dominant Cu-contribution have lower frequencies due to the higher mass; frequencies are particularly low for displacements perpendicular to the Cu-O-bonds. In the lowest optic  $B_{1u}$  mode, Cu atoms neighboring along  $b$  shift almost in the direction of their connection. The mode with the opposite phase corresponds to the lowest  $B_{2u}$ -mode with a significantly lower frequency, 1.4 THz. This pattern allows the O2-atoms to follow the Cu-atoms yielding an almost rigid shift of the ribbons. Also, the tetrahedra are only slightly distorted in this pattern, since they rotate around the  $c$ -axis. In accordance with the two-dimensional character of the  $\text{CuGeO}_3$  lattice<sup>7</sup> this vibration may be considered as the transverse vibration of the zick-zack-planes. This explains the exceptional low frequency of this mode which is related to the low lying longitudinal acoustic  $\Sigma_1$  branch, see below.

The compared experimental and calculated phonon



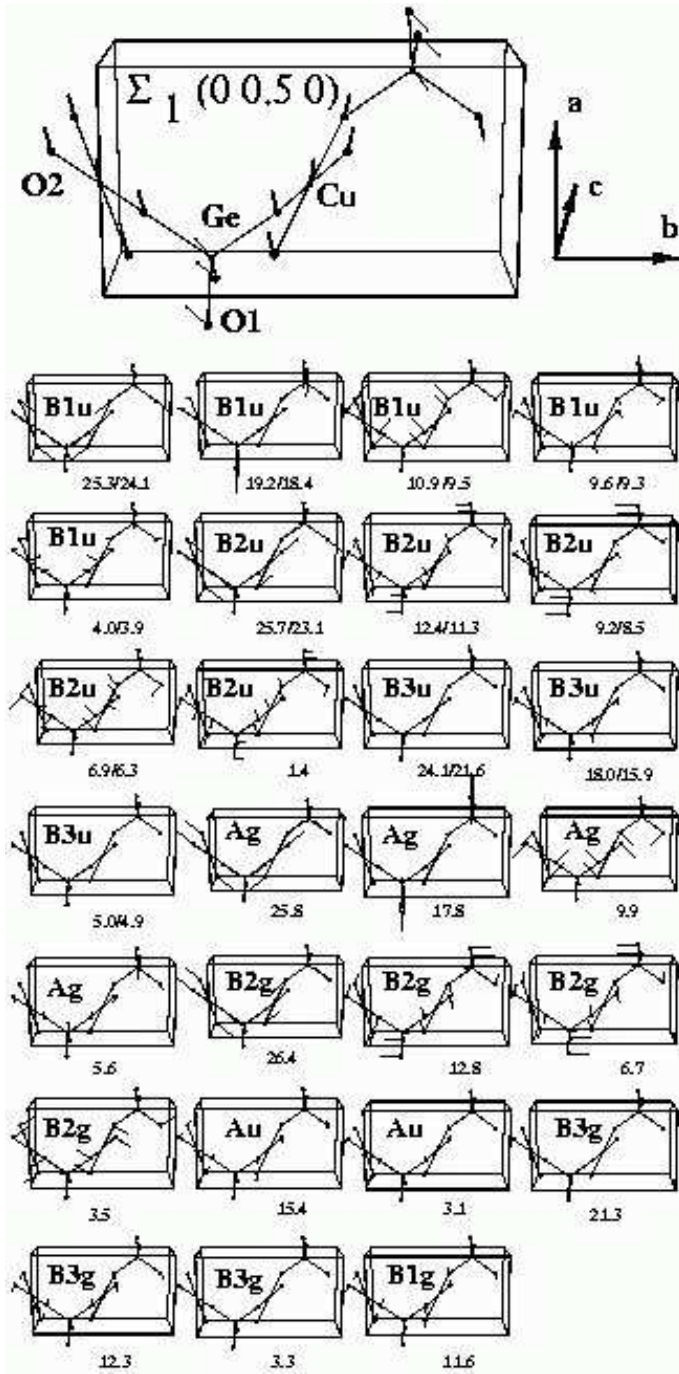


FIG. 4: Polarization patterns of all  $\Gamma$ -modes and their frequencies in THz. The figure on the top illustrates the crystal structure of  $\text{CuGeO}_3$  and gives the polarization pattern of the zone boundary mode of the longitudinal acoustic branch ( $q=(0\ 0.5\ 0)$ ).

dispersion shown in figure 2 indicates strong dispersion mostly in the low frequency range. Furthermore, the curves are steeper along  $c$  than along  $b$  or  $a$ . This reflects the arrangement of the strong bonds, since the phonon dispersion may be considered as the Fourier-transformation of the force constants. The layered structure of  $\text{CuGeO}_3$  has no covalent bonds along  $a$ , therefore, the dispersion stays flat in this direction, at least in the higher frequency range. In consequence, one may expect that also the character of the vibrations does not change in this direction. In contrast, the chain configuration along  $c$  will mix the character in the Brillouin-zone along  $[001]$ .

The dispersion along  $b$  is determined by the coupling between  $\text{CuO}_2$ -ribbons and tetrahedron chains. The glide mirror plane in space group  $\text{Pbmm}$  transforms into the second formula unit in the primitive cell; for vanishing coupling one might separate the zone center modes into modes with the two units vibrating in- or out-of-phase but the finite coupling results in a dispersion along  $b$ . The degeneration of two branches at  $(0\ 0.5\ 0)$  corresponds in most cases to the connection of such a pair. The flat dispersion of many of the branches along  $b$  shows that the coupling is weak for those modes.

In the following we discuss now several particularities of the phonon dispersion in  $\text{CuGeO}_3$  which are not directly related to the spin-Peierls transition.

– *Flat longitudinal acoustic branch along  $b$  and associated modes* – Lorenzo et al. have reported a longitudinal acoustic branch in the  $b$ -direction<sup>14</sup>, which has been interpreted as being essential for the spin-Peierls transition. The low-lying branch has been qualitatively confirmed in later studies<sup>15,16</sup> and also by our own results. However, the results do not agree quantitatively. The low-lying branch may be described within the lattice dynamical model. The low frequencies are explained due to the lowest  $B_{2u}$ -mode. From this mode a  $\Sigma_1$  branch starts, which interacts with the longitudinal acoustic branch of the same symmetry. The character of the acoustic vibration is hence transferred to the optic branch, and the acoustic branch carries the character of the  $B_{2u}$ -mode at 1.5THz, as it is illustrated by the polarization pattern of the zone-boundary acoustic mode, see top of figure 4.

The flat LA branch is hence the consequence of the low-lying optical mode. Similar effects are also seen in the other directions where the lowest  $B_{2u}$ -mode belongs to the  $\Delta_3$ - or  $\Lambda_4$ -representations. The corresponding branch interacts with the transverse acoustic branches,  $\Delta_3$  and  $\Lambda_4$ , respectively.

The flattening was interpreted as indicating direct relevance for the spin-Peierls transition<sup>14</sup>. Damascelli et al.<sup>40</sup> report for the lowest  $B_{2u}$ -mode an anomalous softening upon cooling, which we do not confirm. The polarization pattern of these vibrations, however, has no similarity with the spin-Peierls distortion in  $\text{CuGeO}_3$ . The low frequencies just reflect a structural instability of this material.

The agreement between frequencies obtained by differ-

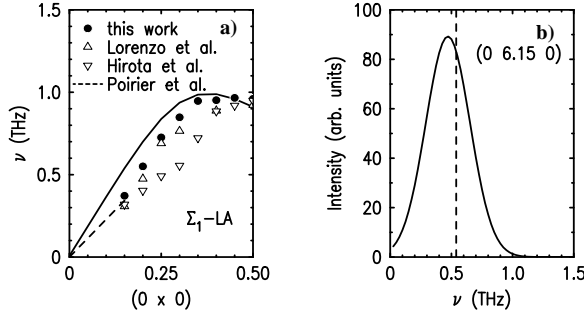


FIG. 5: a) Frequencies of the longitudinal acoustic mode in the  $\Sigma$ -direction; the measured frequencies of this work were corrected for resolution effects. For comparison we also show results of other groups<sup>14,15</sup>. The dashed line corresponds to the linear extrapolation from the elastic constant determined by Poirier et al.<sup>41</sup>, and the solid line to the frequencies calculated with our model. b) Scan calculated by the convolution of the dispersion surface with the spectrometer resolution for  $\mathbf{Q}=(0\ 6.15\ 0)$ ; the exact value of the LA mode frequency at this  $\mathbf{q}$ -value is indicated by the broken line.

ent groups is poor for the LA- $\Sigma_1$ -branch, see figure 5. The convolution of the experimental resolution with the dispersion surface may explain these differences. Figure 5b) shows a scan calculated by the convolution of the experimental resolution (including the mosaic spread of the sample) with the calculated dispersion. By several calculations of this type the resolution-induced correction factors have been determined and applied to the measured frequencies. The corrected frequencies are shown in figure 5. Resolution effects are most likely the origin of the bad agreement between the different neutron results.

– *Soft-mode-behavior* – Figure 6 shows the low energy part of the phonon dispersion of the  $\Lambda_4$ - and  $X0X_2$ -branches. Due to the larger amount of branches of the same symmetry, the interpretation is rendered difficult in the [101]-direction, but one may recognize that the branch starting at the  $B_{2u}$ -mode at 6.3 THz softens continuously through the zone, exhibits several interactions, and ends finally at the lowest zone-boundary frequency. The  $a$ -component does not seem to be relevant for this decrease. As shown in figure 4, the  $B_{2u}$  mode corresponds to a displacement of O2-positions in a square in the same direction coupled with a movement of the Cu-atoms. Along the  $c$ -direction the pattern changes continuously, for  $\mathbf{q}=(0\ 0\ 0.5)$ , O2-O2-edges neighboring along  $c$  are moving in opposite directions, this pattern is shown in figure 7, it may be characterized as a folding of the ribbons. In the following this mode is called soft mode (SM).

The frequency decrease in these branches can be considered as soft-mode behavior; it points to some structural instability, for instance this mode softens by 2.3% upon temperature decrease from 295 to 12 K. This instability in  $\text{CuGeO}_3$  is still far from condensing, but upon substitution or pressure it might become enhanced. The

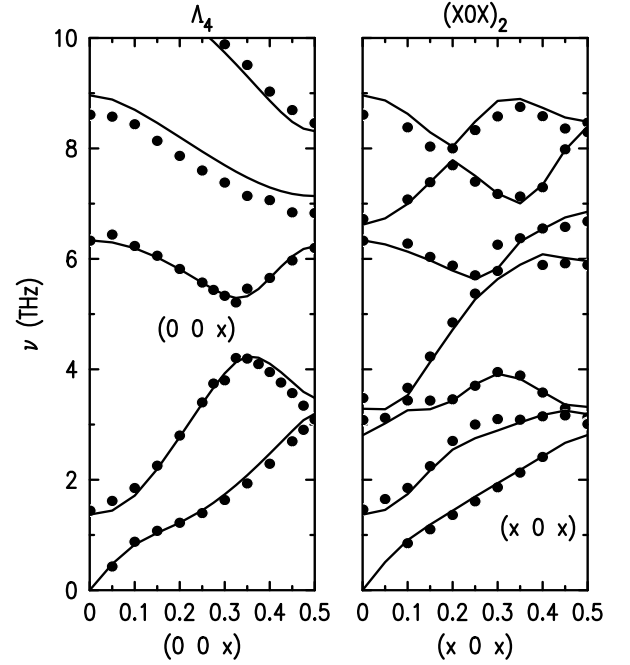


FIG. 6: Part of the dispersion of the  $\Lambda_4$ - and  $X0X_2$ -branches.

SM-instability, however, is not directly related to the spin-Peierls transition.

The  $\Lambda_4$ -mode of similar frequency corresponds to a Cu-shift, see figure 7. The mode with opposite phase between neighboring chains is the  $\Lambda_3$ -mode, in contrast to the corresponding  $\Gamma$ -modes,  $B_{1u}$  and  $B_{2u}$ , the chain coupling only weakly affects the zone-boundary modes.

– *Behavior of the highest Ge-O-branches* – The dispersion of the highest Ge-O-branches is not fully understood. In general the description of these branches by our model is poor due to the insufficient description of the covalent forces, see above. The behavior of the highest  $\Lambda_2$ - and  $X0X_2$ -branches, shown in figures 2 and 11, is surprising. Again, the influence of the  $a$ -component is negligible. The bending down of the branch towards the zone-boundary is reproduced by the model only in general. We do not think that this behavior results from magneto-elastic coupling, but it appears more likely to be an intrinsic property of the tetrahedron chains. "ab-initio" calculations should give more insight into this problem.

– *Further predictions of the lattice dynamical model* – Table VI compares the elastic constants determined by ultra sound and by Brillouin scattering techniques with those calculated by the model. The first ultrasound measurements were limited to the diagonal terms<sup>41,42,43</sup> and a complete set of elastic constants was determined only by Ecollivet et al. using Brillouin scattering<sup>44</sup>. There is some scattering in the experimental data obtained with the ultra-sound techniques. The model values compare best to the combined study in reference<sup>44</sup>. The lattice model predicts  $C_{22}$  to be significantly higher than the experimental value, as may be also seen in figure 6. The

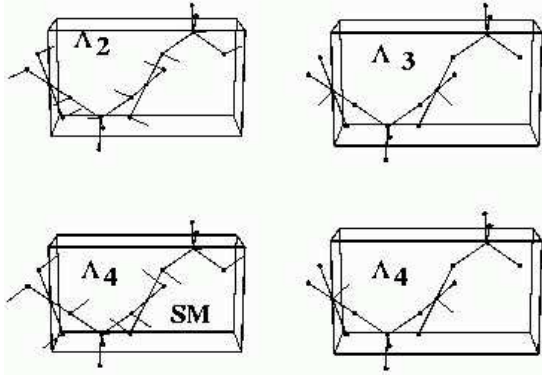


FIG. 7: Polarization-pattern of the four lowest modes at  $\mathbf{q}=(0\ 0\ 0.5)$ .

	c11	c22	c33	c44	c55	c66	c12	c13	c23
US-a	0.624	0.372	3.264	/	/	/	/	/	/
US-b	0.74	0.21	3.32	/	/	/	/	/	/
US-c	0.66	0.345	2.79	/	/	/	/	/	/
US-d	0.71	0.345	3.43	0.37	0.33	0.22	/	/	/
BR	0.64	0.376	3.173	0.353	0.353	0.184	0.321	0.469	0.227
model	0.823	0.500	3.457	0.408	0.435	0.165	0.297	0.403	0.223

TABLE VI: Comparison of the experimentally determined elastic constants (ultra-sound : US-a Poirier et al.<sup>41</sup>, US-b Poirier et al.<sup>42</sup>, US-c Saint-Paul et al.,<sup>43</sup> US-d Ecollivet et al.,<sup>44</sup>; Brillouin scattering : BR Ecollivet et al.,<sup>44</sup>) with those calculated with the lattice dynamical model; elastic constants are given in  $10^{12} \text{ dyn/cm}^2$ .

model seems to slightly underestimate the interaction between the optic and acoustic branches near the zone center. Upon increase of the weight of the LA modes one may obtain better agreement for the elastic constants but at the expense of the description at higher energies, which has been considered to be more relevant.

The phonon density of states, PDOS, has been studied by Arai et al.<sup>45</sup> and by Fujita et al.<sup>46</sup> by inelastic neutron scattering on polycrystalline samples. In figure 8 we show the PDOS weighted with the atomic cross section divided by the mass, the generalized PDOS (GPDOS), calculated with the lattice dynamical model; the agreement with the experiment is at most qualitative. However, the good agreement of the model with the optic frequencies and with the dispersion curves determined here excludes the experimental GPDOS. We think that the deviation results from insufficient correction of multi-phonon processes. Also the strong temperature dependences point to such effects<sup>45,46</sup>. Neither our studies, nor the optical experiments nor the similar work by Nishi et al.<sup>16</sup> give evidence for a strong temperature dependence of the phonon spectrum in  $\text{CuGeO}_3$ . In addition, the measured GPDOS presents huge intensity above the cut-

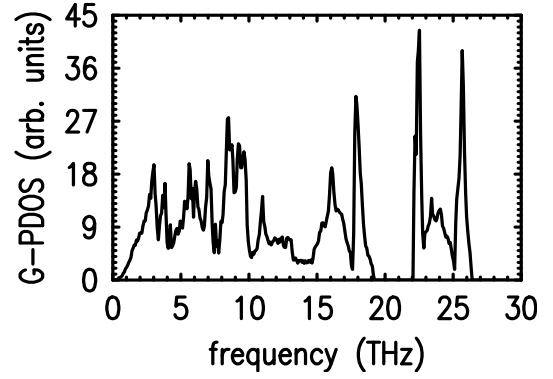


FIG. 8: GPDOS calculated with the lattice dynamical model.

off value of 26 THz, which however, is already fixed by the optics studies.

From the calculated PDOS one may obtain the specific heat at constant volume. Most of the published work on the specific heat deals with the anomaly at the spin-Peierls transition<sup>47,48,49,50</sup>. Only Weiden et al.<sup>50</sup> report a measurement up to room temperature which is compared in figure 9 with the results of the calculations. The difference between specific heat at constant volume and at constant pressure has been corrected empirically, indicated by the solid and dashed lines in figure 9. Since the coefficient of thermal expansion enters the difference in second order, the correction is extremely small, it remains almost in the width of the lines. Surprisingly, the measured specific heat is always about 12% higher than the calculated one; at least at higher temperature this can not be attributed to magnetic contributions. Again, it seems unlikely that the lattice dynamical model is that wrong; for instance the large number of high optic frequencies unambiguously indicate that the specific heat at room temperature is far from its saturation value corresponding to the Dulong-Petit law. A larger specific heat might arise from strong anharmonicity, as in the classic example of  $\text{AgI}$  where a sub-lattice melts<sup>28</sup>. The anharmonicities in  $\text{CuGeO}_3$  appear to be, however, too small for such an explanation.

Another check of the model may be obtained through the comparison with the experimental Debye-Waller factors, see Table VII. The agreement at room temperature is very good, and also the low temperature coefficients, which are more difficult to determine, are well described<sup>7</sup>.

## V. MODES IN RELATION TO THE SPIN-PEIERLS TRANSITION

The structural part of the spin-Peierls transition is characterized by a symmetry reduction in the crystal structure from  $\text{Pbmm}$  to  $\text{Bbcm}$ . The relevant phonon modes may be identified with the help of group theory. In the notation by Stokes and Hatch<sup>52</sup> these modes are

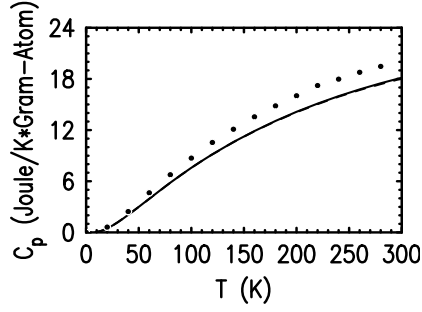


FIG. 9: Comparison of the experimental specific heat (points, taken from reference<sup>50</sup>) with the calculated ones; the solid line corresponds to  $c_p$  and the dashed one to  $c_v$ .

atom	exp.	cal.	atom	exp.	cal.
Ge-U11	70(3)	55	O1-U11	81(4)	64
-U22	101(3)	90	-U22	129(4)	117
-U33	40(3)	31	-U33	48(3)	42
Cu-U11	115(3)	100	O2-U11	144(3)	127
-U22	142(2)	116	-U22	178(3)	161
-U33	46(3)	42	-U33	61(3)	56
-U12	50(2)	37	-U12	79(2)	69

TABLE VII: Debye-Waller-coefficients in  $\text{CuGeO}_3$  at room temperature : comparison of experimental (average of x-ray and neutron results from<sup>6</sup>) and calculated values, in  $10^{-4} \text{\AA}^2$ .

labeled  $T_2^+$  at  $\mathbf{q}=(0.5 \ 0 \ 0.5)$ , The  $T_2^+$ -modes are characterized by four independent parameters in their polarization pattern which reflect the four additional structural parameters in the dimerized structure. The corresponding irreducible representation is one-dimensional and has a multiplicity of four. The  $T_2^+$ -modes have been discussed in detail in references<sup>12,17</sup> including their temperature dependence. In this section we want to give some further information on the dispersion of the branches connected to these four modes directly involved. The lowest  $T_2^+$ -mode at 3.12 THz is  $B_{2g}$ -like associated with a rotation of the O2-O2-edges around the  $c$ -axis; it modulates the O2-O2-Ge angle,  $\delta$ , and, therefore, also the magnetic interaction  $J$ . The second lowest mode at 6.53 THz is associated with the modulation of the Cu-O2-Cu bond angle  $\eta$ , which determines strongest the magnetic interaction. This  $\eta$ -mode seems to be the one most important for the spin-Peierls transition. The higher frequency  $T_2^+$ -modes at 11 and 25 THz correspond to the Cu-O2- and Ge-O bond stretching and are less relevant for the spin-Peierls transition. The  $T_2^+$ -representation corresponds to the propagation vector of  $\mathbf{q}=(0.5 \ 0 \ 0.5)$ , therefore, it is interesting to analyze the dispersion in the  $[101]$ -direction, see figure 11.

–  $[101]$ -direction and identification of the relevant modes – The  $\Gamma$ -modes whose polarization patterns are closest to the structural distortion in the spin-Peierls

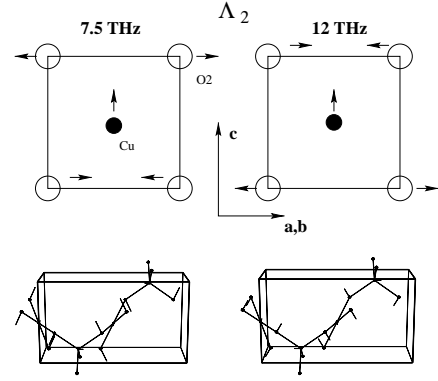


FIG. 10: Polarization patterns of the two modes with Cu-shift along  $c$  at  $\mathbf{q}=(0 \ 0 \ 0.5)$ ; the upper two pictures show a projection of a single  $\text{CuO}_4$ -square.

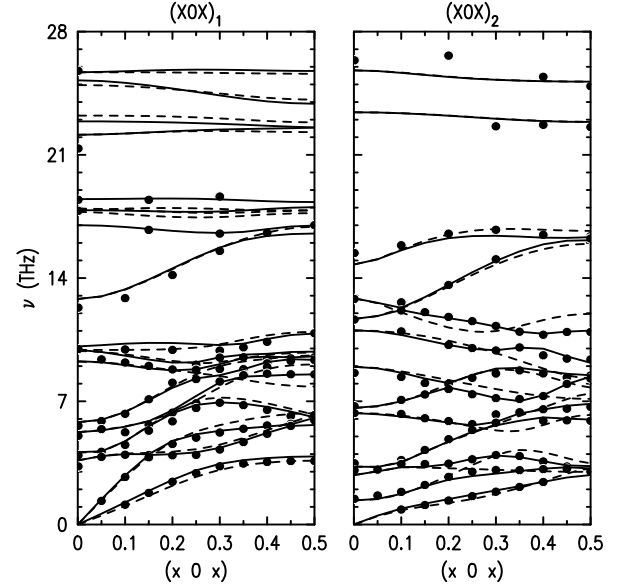


FIG. 11: Dispersion of the branches in the  $[101]$ -direction. The symbols denote measured frequencies and the solid lines those calculated by the lattice dynamical model. Dashed lines denote the dispersion of corresponding  $\Lambda$ -branches neglecting the influence of the  $a^*$ -component.

phase are the  $A_u$  and  $B_{2g}$ -modes where branches of  $\Lambda_2$ -symmetry start in the  $\Lambda$ -direction. As may be seen in the polarization schemes given in Table I, the  $\Lambda_2$ -representation allows the  $z$ -shift of Cu and the  $x, y$ -shifts for O2. These Cu and O-characters of these modes are well separated near the zone center but they mix in the zone. Along the  $[101]$ -direction the modes may be divided only according to two different representations, 17  $X_0X_1$ - and 13  $X_0X_2$ -modes. The large number of modes of the same symmetry renders the interpretation of the data rather difficult. The compatibility relations show that the  $T_2^+$ -modes correspond to the zone-boundary modes

of the  $X0X_2$ -branches, see Table I.

At the zone-boundary (0 0 0.5) there are two vibrations where the Cu moves along  $c$ , the upper one is isolated in frequency near 12 THz and the lower one near 7.7 THz. As may be seen in figure 10, the difference in these modes consists in the phases of Cu and O2-displacements. In the higher mode, Cu moves towards the shorter O2-O2-edge yielding a strong alternation of the Cu-O-bond lengths and, therefore, the higher energy. In contrast, for the lower mode Cu shifts towards the longer edge yielding an alternation of the bond angle. Besides the  $a$ -component this movement represents the main part of the structural distortion in the dimerized phase. These modes are called  $\eta$ -modes in the following.

The  $B_{2g}$ -mode near 3.5 THz corresponds to the rotation of the edges of the  $\text{CuO}_4$ -squares and hence to the second dominant feature of the spin-Peierls distortion. A flat  $\Lambda_2$ -branch is starting at this mode, which ends at the zone-boundary at a mode with opposite twisting of edges neighboring along  $c$ . Again, only the  $a$  component is missing for the description of the distortion in the dimerized phase. In general one may arrive at the relevant  $T_2^+$ -modes by either analyzing the path from (0 0 0.5) to (0.5 0 0.5) where there is only little dispersion or studying the [101]-dispersion, see below and reference<sup>17</sup>.

Figure 11 shows the phonon dispersion in the [101]-direction. Again the dispersion is well described by the model. From the compatibility relation in Table II one recognizes that  $X0X_1$ -branches correspond to the combination of  $\Lambda_1$ - and  $\Lambda_3$ -branches in the [001]-direction, and  $X0X_2$ -branches correspond to  $\Lambda_2$ - and  $\Lambda_4$ -branches. In figure 11 we show the corresponding  $\Lambda$ -branches as broken lines neglecting the  $x$ -component of the wave-vector (i.e. in a projection). The resemblance shows that the  $a^*$ -component influences the frequencies only slightly, in agreement with the flat dispersion along  $a$  and the lack of any covalent bond in this direction. However, the influence of the  $a^*$ -component may not at all be neglected for the interpretation of the intensities. Along the  $\Lambda$ -direction one observes only  $\Lambda_1$ -branches at  $\mathbf{Q}=(0\ 0\ 2+x)$ ; the intensities of  $\Lambda_3$ -modes are suppressed, similar to an elastic extinction rule. In the [101]-direction, however, one may also observe the  $X0X_1$ -modes corresponding to the  $\Lambda_3$ -modes at  $\mathbf{Q}=(x\ 0\ 2+x)$  with comparable intensities. The observation that structure factors are much more sensitive than the intensities corresponds to the experience with small structural distortions<sup>51</sup>.

Due to the larger number of modes of same symmetry the mixing of the characters is even more important in the [101]-direction. Nevertheless, it has been possible to clearly identify the  $T_2^+$ -modes at  $b\Gamma_q=(0.5\ 0\ 0.5)$  in reference<sup>17</sup>. The  $T_2^+$ -mode rotating the O2-edges is found at 3.12 THz, the most relevant  $\eta$ -modulating mode at 6.53 THz, and the two highest  $T_2^+$ -modes exhibit frequencies of 11.2 and 24.9 THz, respectively, see reference<sup>17</sup>.

– *Comparison with Raman-studies in the dimerized phase*– Raman-studies below  $T_{SP}$  have been very early performed by Udagawa et al.<sup>32</sup> and by Sugai

et al.<sup>53</sup>; they show additional peaks in the spin-Peierls phase. In the meanwhile there have been many publications on these intensities, which agree concerning the experimental findings but not on the interpretation<sup>32,53,54,55,56,57,58,59,60,61,62</sup>. All groups find five additional peaks; additional much weaker intensities are reported in reference<sup>58,61</sup> and appear to arise from some different mechanism.

The lowest intensity near  $30\text{cm}^{-1}$  is of magnetic origin. All Raman-interpretations agree that the highest two strong peaks correspond to folded phonons, they perfectly agree to our results on the two highest  $T_2^+$ -modes. But also the two peaks at lower frequencies which were interpreted controversially may be identified as  $T_2^+$ -modes, since their frequencies perfectly agree with those of the  $B_{2g}$ -like and  $\eta$ -  $T_2^+$ -modes. The neutron scattering studies reveal a strong broadening of the  $\eta$ -mode in good agreement with the Raman-experiments; Lemmens et al.<sup>60</sup> report a width of  $16\text{cm}^{-1}$ . In addition, it has been found that just the Raman-intensity corresponding to the  $\eta$ -mode can be observed a few degrees K above the spin-Peierls transition.<sup>60,61</sup> This underlines once more the exceptional role of the  $\eta$ -mode in the spin-Peierls transition.

– *Dispersion of the branches connected to the  $T_2^+$ -modes* – In general the dispersion is rather flat along the  $a$ -direction. This is also valid for branches starting at the  $T_2^+$ -modes and passing along the path (0.5- $x$  0 0.5) on the zone boundary. The endpoint corresponds to the zone-boundary of the  $\Lambda$ -direction. The small influence of the  $a^*$ -component is already illustrated in figure 11 and was used to discuss the character of the  $T_2^+$ -modes. The modes at  $\mathbf{q}=(0\ 0\ 0.5)$  may be further divided according to symmetry. In particular, there is a representation of multiplicity four which corresponds to the  $T_2^+$ -modes at (0.5 0 0.5). The frequencies of these four modes lie at 3.29, 7.69, 12.1 and 24.9 THz, compared to the  $T_2^+$ -frequencies at 3.12, 6.53, 11.2 and 24.9 THz at room temperature.

The (0 0 0.5)-mode corresponding to the  $B_{2g}$ -like  $T_2^+$ -mode turning the O2-edges is only slightly harder than the  $T_2^+$ -mode, at room temperature. At low temperature, the difference is even smaller since the (0 0 0.5)-mode hardens slightly to 3.34 THz, whereas the  $T_2^+$ -mode is significantly shifted due to the magneto-elastic coupling<sup>17</sup>.

The difference in frequency for the modes modulating the Cu-O-Cu-bond angle,  $\eta$ , the main feature of the spin-Peierls distortion in  $\text{CuGeO}_3$ , is more pronounced, about 1 THz. This dispersion explains the doubling of the lattice in the  $a$ -direction; the distortion with modulation along  $a$  just requires less structural energy. For these  $\eta$ -modes too, the stronger frequency increase upon cooling is observed for  $\mathbf{q}=(0.5\ 0\ 0.5)$ ; but also the (0 0 0.5)-mode frequency increases significantly, by 1.5%.

The second highest  $T_2^+$ -mode exhibits a significant frequency increase towards (0 0 0.5), whereas the Ge-O-modes are little influenced by the  $a^*$ -component.

The dispersion along the  $b$ -direction on the zone-



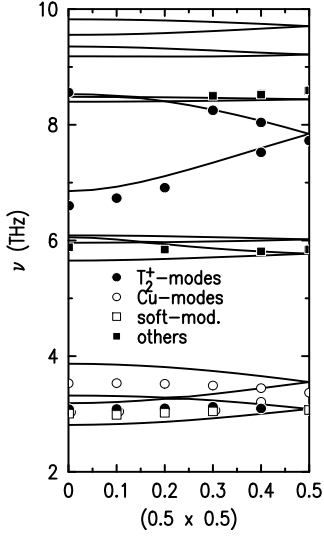


FIG. 12: Dispersion of branches connected to the  $T_2^+$ -modes along the path  $(0.5 \times 0.5)$  at room temperature ; symbols denote experimental frequencies and lines calculations.

boundary  $(0.5 \times 0.5)$  is comparable to that in the  $\Sigma$ -direction. In particular, there is a degeneration of two modes at  $(0.5 \ 0.5 \ 0.5)$ . Again, two  $(0.5 \ 0 \ 0.5)$ -modes connect which correspond to the phase shift between the two formula units. Figure 12 shows the dispersion along this path, and figure 13 indicates the polarization patterns of several  $(0.5 \ 0 \ 0.5)$ -modes relevant for the following discussion.

There are four modes in the range 3–4 THz at  $\mathbf{q}=(0.5 \ 0 \ 0.5)$ : the  $T_2^+$ -mode, two Cu-modes, associated to the lowest optic  $B_{1u}$ - and  $B_{2u}$ -frequencies and the soft mode. As in the  $\Sigma$ -direction, the two Cu-modes connect. For the  $T_2^+$ -mode the situation is more complicated : considering the scheme of a single  $\text{CuO}_2$ -ribbon, one might expect an opposite-phase mode, where along  $b$  neighboring O2-O2-edges rotate in the same sense concerning their angle to the  $a$ -axis. This movement, however, would result in a strong modulation of the Ge-O-bonds causing much higher frequency. On the contrary one may consider this  $T_2^+$ -mode as a rotation of the  $\text{GeO}_4$ -tetrahedra around the O1-O1-line. In the  $T_2^+$ -mode two tetrahedra neighboring along  $b$  turn both clockwise or both anti-clockwise; the movement with different phase – one clockwise the other anti-clockwise – results in a completely different displacement scheme concerning the  $\text{CuO}_2$ -ribbons, since both O2-positions in an O2-O2-edge perpendicular to  $c$  move then in the same direction. This pattern corresponds to the soft mode at  $(0.5 \ 0 \ 0.5)$ , see figure 13. The lowest  $T_2^+$ -mode connects hence with the soft mode along the  $b$ -direction but loses the modulation of the magnetic interaction along this path. The anomalous frequency increase upon cooling<sup>17</sup> observed for the  $T_2^+$ -mode has been followed along  $b^*$ ; the frequency hardening continuously decreases till  $(0.5 \ 0.5 \ 0.5)$ ; in contrast the soft-mode even

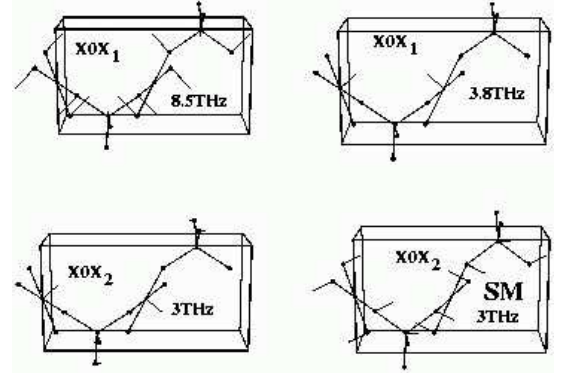


FIG. 13: Polarization patterns of four modes at  $\mathbf{q}=(0.5 \ 0 \ 0.5)$ , which are related to the  $T_2^+$ -modes at 6.6 THz ( $\eta$ -mode) and at 3.1 THz ( $B_{2g}$ -like mode).

softens by 2.3(3) % upon cooling from room temperature to 12 K.

For the  $\eta$ -mode the Ge-O-forces do not play an important role; therefore, one may easily follow these modes along  $b^*$ . One finds a significant frequency enhancement; the corresponding mode is found at 8.56 THz, its polarization pattern, see figure 13, exhibits a smaller Cu-displacement than that of the  $T_2^+$ - $\eta$ -mode. In the range 5-6 THz, there are several flat branches included in figure 12 which are not related to the spin-Peierls distortion. The temperature dependence of the bond angle modulating modes close to  $(0.5 \ 0 \ 0.5)$  could not be studied, since in this region additional magnetic intensity appears upon cooling<sup>64</sup>. For  $q_b=0.5$  no temperature dependence has been detected, also the intensities near 5.8 THz are almost temperature independent.

The dispersion of the branches connected to the two lower  $T_2^+$ -modes explains the propagation vector of the structural distortion in the spin-Peierls phase,  $\mathbf{q}=(0.5 \ 0 \ 0.5)$ . The  $b$ -component is fixed through the Ge-O-forces, which shift the mode rotating the O2-O2-edges to very high energies and which also cause a sizeable slope of the  $\eta$ -modulating branch. The weaker inter-plane forces lead to the doubling of the  $a$ -parameter mainly due to their influence on the  $\eta$ -modes. The structural distortion involved in the spin-Peierls transition has, therefore, a clear three-dimensional character. Therefore, a RPA treatment of the spin-phonon coupling in the transition appears to be justified<sup>12</sup>.

The dispersion of the phonon branches should reflect the extension of the critical scattering along the three orthorhombic directions. In a classical soft-mode transition one may expand the frequency of the involved mode at the propagation vector of the structural distortion,  $\mathbf{q}_0$ , here  $(0.5 \ 0 \ 0.5)$  with  $\mathbf{q} = \mathbf{q}_0 + \mathbf{q}_a + \mathbf{q}_b + \mathbf{q}_c$  :

$$\omega(\mathbf{q}) = \omega_0 + c_a \cdot \mathbf{q}_a^2 + c_b \cdot \mathbf{q}_b^2 + c_c \cdot \mathbf{q}_c^2 \quad (4).$$

Linear terms do not exist, since there must be a fre-

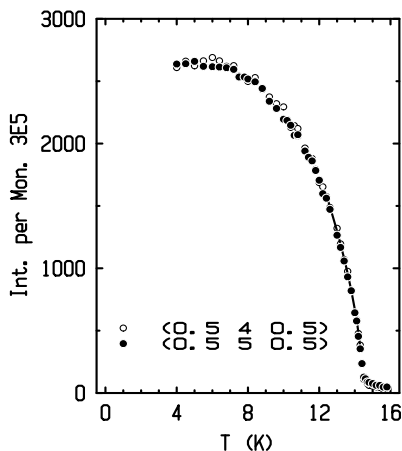


FIG. 14: Intensity of the two superstructure reflections at  $\mathbf{Q}=(0.5\ 3\ 0.5)$  and  $(0.5\ 4\ 0.5)$  as function of temperature. The two intensities reflect approximately the distortion of the two lowest  $T_2^+$ -modes. The line corresponds to a fit by power law.

quency minimum at  $\mathbf{q}_0$ . The ratio of the constants  $c_a, c_b, c_c$  should correspond to the ratio of the correlation lengths of critical scattering in the three directions. In  $\text{CuGeO}_3$  this analysis is not obvious since there is no softening and since at least the correlation length along  $c$  is dominated by the magnetic interaction. Furthermore, the fitting of the experimental dispersion by a quadratic expansion is not very satisfactory; one obtains  $c_a = 2.6\ \text{THz}/\text{\AA}^2$ ,  $c_b = 8.0\ \text{THz}/\text{\AA}^2$  and  $c_a/c_b = 0.3$ , for the  $\eta$ -mode which is the most relevant one.

The observed correlation lengths decrease very rapidly above the transition; only a few degrees K above it they amount to a few lattice constants; therefore, rather large  $\mathbf{q}_a$  and  $\mathbf{q}_b$ -values are involved, where a quadratic expansion is certainly no longer valid. Nevertheless, the ratio between the correlation lengths determined by Schoeffel et al.<sup>65</sup>  $\frac{\xi_a}{\xi_b} \sim 1/4$  may be qualitatively explained by the dispersion of the branches around the  $T_2^+$ - $\eta$ -mode.

## VI. POSSIBILITY OF INDEPENDENT ORDER PARAMETERS

Since the structural distortion in the spin-Peierls phase does not correspond to a single phonon Eigen-mode, one might speculate whether the low temperature phase is described by a single order parameter or whether more than one parameters are needed in order to describe the temperature dependence of the distortion. We have analyzed this problem by measuring two superstructure re-

flections which are not sensitive to the same features of the distortion. Intensity at  $(0.5\ 3\ 0.5)$  is mainly related to the distortion corresponding to the lowest  $T_2^+$ -mode with  $B_{2g}$ -character, and intensity at  $(0.5\ 4\ 0.5)$  reflects the  $\eta$ -modulation. In spite of their different sensitivities these two super-structure exhibit exactly the same temperature dependence as it is shown in figure 14. Fitting a critical behavior,  $I \propto (T_{SP} - T)^{2\beta}$ , to the temperature dependence of these superstructure intensities yields a critical exponent of  $\beta = 0.30(1)$  in good agreement with previous results<sup>66,67,68</sup> and in particular with the thermal expansion study<sup>9</sup>. The scaling between the two superstructure reflections remains also valid slightly above the spin-Peierls transition, indicating that the whole structural transition may be described by a single order-parameter.

## VII. CONCLUSION

The various inelastic neutron scattering studies have yielded a detailed understanding of the lattice dynamics in  $\text{CuGeO}_3$ . The developed model not only describes the observed dispersion curves, but it allows the interpretation of Raman and infrared-frequencies, elastic constants and anisotropic Debye-Waller parameters. It further predicts the PDOS and the phononic part of the specific heat, on which only little experimental information exists till today.

Only the extensive study of the phonon dispersion has allowed the identification of those modes directly involved in the transition<sup>17</sup>. The dispersion of the branches connecting with these modes clearly explains the occurrence of the structural transition at  $\mathbf{q}=(0.5\ 0\ 0.5)$ , since the phonon frequencies of modes modulating the bond-angle  $\eta$  are lowest at this  $\mathbf{q}$ -value. The pronounced dispersion of the phonon branches involved in the spin-Peierls transition clearly illustrate a three-dimensional character of the structural part of the transition. The influence of the magneto-elastic coupling on the temperature dependence of phonon frequencies should occur not only in  $\text{CuGeO}_3$  but also in materials with related structure, like for example the spin-ladder compounds.

$\text{CuGeO}_3$  is amongst the most complex materials where the phonon dispersion has been analyzed in that detail. It appears therefore to be a promising candidate for the extension of current “ab initio” techniques to complex materials.

**Acknowledgments.** Work at Cologne University was supported by the Deutsche Forschungsgemeinschaft through the Sonderforschungsbereich 608.

\* electronic mail : braden@ph2.uni-koeln.de

<sup>1</sup> M. Hase, I. Terasaki and K. Uchinokura. *Phys. Rev. Lett.*, 70:3651, 1993.

<sup>2</sup> J.P. Pouget, L.P. Regnault, M. Aïn, B. Hennion, J.P. Renard, P. Veillet, G. Dhalenne and A. Revcolevschi. *Phys.*

- Rev. Lett.*, 72:4037, 1994.
- <sup>3</sup> L.P. Regnault, M. Aïn, B. Hennion, G. Dhalenne and A. Revcolevschi. *Phys. Rev.*, B53:5579, 1996.
  - <sup>4</sup> K. Hirota, D.E. Cox, J.E. Lorenzo, G. Shirane, J.M. Tranquada, M. Hase, K. Uchinokura, H. Kojima, Y. Shibuya and I. Tanaka. *Phys. Rev. Lett.*, 73:736, 1994.
  - <sup>5</sup> H.K. Müller-Buschbaum. *Angew. Chem. Int. Ed. Engl.*, 28:1472, 1989.
  - <sup>6</sup> M. Braden, G. Wilkendorf, J. Lorenzana, M. Aïn, G.J. McIntyre, M. Behruzi, G. Heger, G. Dhalenne and A. Revcolevschi. *Phys. Rev.*, B54:1105, 1996.
  - <sup>7</sup> M. Braden, E. Ressouche, B. Büchner, R. Keßler, G. Heger, G. Dhalenne and A. Revcolevschi. *Phys. Rev.*, B57:11497, 1998.
  - <sup>8</sup> W. Geertsma and D. Khomskii. *Phys. Rev.*, B54:3011, 1996.
  - <sup>9</sup> H. Winkelmann, E. Gamper, B. Büchner, M. Braden, A. Revcolevschi and G. Dhalenne. *Phys. Rev.*, B51:12884, 1995.
  - <sup>10</sup> S. Feldkemper and W. Weber. *Phys. Rev.*, B62:3816, 2000.
  - <sup>11</sup> B. Büchner, H. Fehske, A. Kampf and G. Wellein. *Preprint cond-mat/9806022*, 1998.
  - <sup>12</sup> R. Werner, C. Gros and M. Braden. *Phys. Rev.*, B59:14356, 1999.
  - <sup>13</sup> Z.V. Popović, S.D. Dević, V.N. Popov, G. Dhalenne and A. Revcolevschi. *Phys. Rev.*, B52:4185, 1995.
  - <sup>14</sup> J.E. Lorenzo, H. Hirota, G. Shirane, J.M. Tranquada, M. Hase, K. Uchinokura, H. Kojima, I. Tanaka and Y. Shibuya. *Phys. Rev.*, B50:1278, 1994.
  - <sup>15</sup> K. Hirota, R.J. Birgeneau, M. Hase, H. Kojima, J.E. Lorenzo, Y. Shibuya, G. Shirane, I. Tanaka, J.M. Tranquada and K. Uchinokura. *Physica*, B213&214:284, 1995.
  - <sup>16</sup> M. Nishi, O. Fujita and J. Akimitsu. *Physica*, 210:149, 1995.
  - <sup>17</sup> M. Braden, B. Hennion, W. Reichardt, G. Dhalenne and A. Revcolevschi. *Phys. Rev. Lett.*, 80:3634, 1998.
  - <sup>18</sup> M. Cross and D.S. Fisher. *Phys. Rev.*, B19:402, 1979.
  - <sup>19</sup> C. Gros and R. Werner. *Phys. Rev.*, B58:R14677, 1998.
  - <sup>20</sup> G.S. Uhrig. *Phys. Rev.*, B57:R14004, 1998.
  - <sup>21</sup> R.J. Bursill, R.H. McKenzie and C.J. Hammer, *Phys. Rev. Lett.*, 83:408, 1999.
  - <sup>22</sup> G. Wellein, H. Fehske and A.P. Kampf, *Phys. Rev. Lett.*, 81:3956, 1998.
  - <sup>23</sup> F. Liebau. *Structural Chemistry of Silicates*. Springer Verlag, Berlin, 1985.
  - <sup>24</sup> Laboratoire Léon Brillouin. Equipments experimentaux, 1995. Laboratoire Léon Brillouin, CE-Saclay.
  - <sup>25</sup> L. Pintschovius. *Nuclear Instruments and Methods in Physics Research A*, 338:136, 1994.
  - <sup>26</sup> G.L. Squires. *Thermal Neutron Scattering*. Cambridge University Press, Cambridge, (1978).
  - <sup>27</sup> D.L. Rousseau, R.P. Bauman and S.P.S. Porto. *J. Raman Spectrosc.*, 10:253, 1981.
  - <sup>28</sup> P. Brüesch. *Phonons : Theory and Experiments : I*. Springer Verlag, Berlin Heidelberg New-York, (1982).
  - <sup>29</sup> P. Brüesch. *Phonons : Theory and Experiments : II*. Springer Verlag, Berlin Heidelberg New-York, (1982).
  - <sup>30</sup> S.L. Chaplot, W. Reichardt, L. Pintschovius and N. Pyka. *Phys. Rev.*, B52:7230, 1995.
  - <sup>31</sup> W. Reichardt. Genax-program for lattice dynamical calculations, unpublished.
  - <sup>32</sup> M. Udagawa, H. Aoki, N. Ogita, O. Fujita, A. Sohma, A. Ogihara and J. Akimitsu. *Journal of the Physical Society of Japan*, 63:4060, 1994.
  - <sup>33</sup> S.D. Dević, M.J. Konstantinović, Z.V. Popović, G. Dhalenne and A. Revcolevschi. *J. Phys. - Condens. Matter*, 6:L745, 1994.
  - <sup>34</sup> D.A. Adams and P.A. Fletcher. *Spectrochimica Acta*, 44A:233, 1988.
  - <sup>35</sup> N.E. Massa, J. Campá and I. Rasines. *Phys. Rev.*, B52:15920, 1995.
  - <sup>36</sup> P.H.M. van Loosdrecht, S. Huant, G. Martinez, G. Dhalenne and A. Revcolevschi. *Phys. Rev.*, B54:R3730, 1996.
  - <sup>37</sup> G. Li, J.L. Musfeldt, Y.J. Wang, S. Jandl, M. Poirier, A. Revcolevschi, and G. Dhalenne. *Phys. Rev.*, B54:R15633, 1996.
  - <sup>38</sup> A. Damascelli, D. van der Marel, F. Parmigiani, G. Dhalenne and A. Revcolevschi. *Preprint*, 1998.
  - <sup>39</sup> J.J. McGuire, T. Room, T.E. Mason, T. Timusk, H. Dabkowska S.M. Coad and D. McK.Paul. *Preprint cond-mat/9707163*, 1997.
  - <sup>40</sup> D. Damascelli, D. van der Marel F. Parmigiani, G. Dhalenne and A. Revcolevschi. *Phys. Rev.*, B56:11373, 1997.
  - <sup>41</sup> M. Poirier, M. Castonguay, A. Revcolevschi and G. Dhalenne. *Phys. Rev.*, B52:16058, 1995.
  - <sup>42</sup> M. Poirier, M. Castonguay, A. Revcolevschi and G. Dhalenne. *Phys. Rev.*, B51:6147, 1995.
  - <sup>43</sup> M. Saint-Paul, G. Remenyi, N. Hegmann, P. Monceau G. Dhalenne and A. Revcolevschi. *Phys. Rev.*, B52:15298, 1995.
  - <sup>44</sup> C. Ecolivet, M. Saint-Paul, G. Dhalenne and A. Revcolevschi. *J. Phys. : Condens. Matter* 11, 4157 (1999).
  - <sup>45</sup> M. Arai, M. Fujita, K. Ubukata, T. Bokui, K. Tabata, H. Ohta, M. Motokawa, T. Otoma, K. Ohyama, M. Mino, J. Akimitsu and O. Fujita. *Journal of the Physical Society of Japan*, 63:1661, 1994.
  - <sup>46</sup> M. Fujita, K. Ubukata, M. Arai, T. Tonegawa, M. Mino, M. Motokawa, K. Knight, B. Forsyth, S.M. Bennington, J. Akimitsu and O. Fujita. *Physica*, B219&220:95, 1996.
  - <sup>47</sup> H. Kuroe, K. Kobayashi, T. Sekine, M. Hase, Y. Sasago, I. Terasaki and K. Uchinokura. *Journal of the Physical Society of Japan*, 63:365, 1994.
  - <sup>48</sup> S. Sahling, J.C. Lasjaunias, P. Monceau and A. Revcolevschi. *Sol. State Commun.*, 92:423, 1994.
  - <sup>49</sup> X. Liu, J. Wosnitza, H.v. Löhneysen and R.K. Kremer. *Z. Physik B - condensed matter*, 98:163, 1995.
  - <sup>50</sup> M. Weiden, J. Köhler, G. Sparr, M. Köppen, M. Lang, C. Geibel, and F. Steglich. *Z. Physik B - condensed matter*, 98:167, 1995.
  - <sup>51</sup> W. Reichardt and M. Braden, *Physica* B263-264, 416 (1999).
  - <sup>52</sup> H. T. Stokes and D. M. Hatch. *Isotropy Subgroups of the 230 Crystallographic Space Groups*. World Scientific, Singapore, 1988.
  - <sup>53</sup> S. Sugai. *Journal of the Physical Society of Japan*, 62:3829, 1993.
  - <sup>54</sup> H. Kuroe, T. Sekine, M. Hase, Y. Sasago, K. Uchinokura, H. Kojima, I. Tanaka and Y. Shibuya. *Phys. Rev.*, B50:16468, 1994.
  - <sup>55</sup> N. Ogita, Y. Tsunazumi, H. Aoki, M. Udagawa, O. Fujita, A. Ogihara and J. Akimitsu. *Physica*, B219&220:107, 1996.
  - <sup>56</sup> H. Kuroe, J. Sasaki, T. Sekine, Y. Sasago, M. Hase, N. Koide, K. Uchinokura, H. Kojima, I. Tanaka and Y. Shibuya. *Physica*, B219&220:104, 1996.
  - <sup>57</sup> C. Gros, W. Wenzel, A. Fledderjohann, P. Lemmens, M. Fischer, G. Güntherodt, M. Weiden, C. Geibel and F.



- Steglich. *Phys. Rev.*, B55:15048, 1997.
- <sup>58</sup> I. Loa, S. Gronemeyer, C. Thomsen and R.K. Kremer. *Sol. State Commun.*, 99:231, 1996.
- <sup>59</sup> P.H.M. van Loosdrecht, J.P. Boucher, G. Martinez, G. Dhalenne and A. Revcolevschi. *Phys. Rev. Lett.*, 76:311, 1996.
- <sup>60</sup> P. Lemmens, B. Eisener, M. Brinkmann, L.V. Gasparow, G. Güntherodt, P. van Dongen, W. Richter, M. Weiden, C. Geibel and F. Steglich. *Physica*, B223&224:535, 1996.
- <sup>61</sup> N. Ogita, T. Minami, Y. Tanimoto, O. Fujita, J. Akimitsu, P. Lemmens, G. Güntherodt and M. Udagawa. *Journal of the Phys. Soc. of Jp.*, 62:3754, 1996.
- <sup>62</sup> V.N. Muthukumar, C. Gros, R. Valenti, M. Weiden, C. Geibel, F. Steglich, P. Lemmens, M. Fischer and G. Güntherodt. *Phys. Rev.*, B55:5944, 1997.
- <sup>63</sup> P.H.M. van Loosdrecht, J. Zeman, G. Martinez, G. Dhalenne and A. Revcolevschi. *Phys. Rev. Lett.*, 78:487, 1997.
- <sup>64</sup> M. Braden, B. Hennion, P. Pfeuty, G. Dhalenne and A. Revcolevschi. *Phys. Rev. Lett.*, 83:1858, 1999.
- <sup>65</sup> J.P. Schoeffel, J.P. Pouget, G. Dhalenne and A. Revcolevschi. *Phys. Rev.*, B53:14971, 1996.
- <sup>66</sup> Q. J. Harris, Q. Feng, R.J. Birgeneau, K. Hirota, K. Kakurai, J.E. Lorenzo, G. Shirane, M. Hase, K. Uchinokura, H. Kojima, I. Tanaka und Y. Shibuya. *Phys. Rev.*, B50:12606, 1994.
- <sup>67</sup> Q.J. Harris, Q. Feng, R.J. Birgeneau, K. Hirota, G. Shirane, M. Hase und K. Uchinokura. *Phys. Rev.*, B52:15420, 1995.
- <sup>68</sup> M.D. Lumsden, B.D. Gaulin, H. Dabrowska und M.L. Plummer. *Phys. Rev. Lett.*, 76:4619, 1996.